

Analía N. Cillis · Olaf Reimer · Diego F. Torres.

Gamma-ray source stacking analysis at low galactic latitudes

Received: date / Accepted: date

Abstract We studied the problematic of uncertainties in the diffuse gamma radiation apparent in stacking analysis of EGRET data at low Galactic latitudes. Subsequently, we co-added maps of counts, exposure and diffuse background, and residuals, in varying numbers for different sub-categories of putatively and known source populations (like PSRs). Finally we tested for gamma-ray excess emission in those maps and attempt to quantify the systematic biases in such approach. Such kind of an analysis will help the classification processes of sources and source populations in the GLAST era.

Keywords gamma rays · observations · pulsars · methods: data analysis

PACS 95.85.Pw · 98.70.Rz · 97.60.Gb · 95.75.-z

1 Introduction

The EGRET era fades away while the Large Area Telescope onboard GLAST is in its final stages of hardware integration. Many unidentified gamma-ray sources

are still unidentified, especially at low galactic latitudes, where, for instance, not a single supernova remnant could be unambiguously detected (e.g., [1]). Stacking techniques are then a powerful tool to explore, in conjunction with spatial cross-localization of sources followed up by Monte Carlo analysis (e.g., [2]), if populations as a whole arise in the data. The difficulty being, of course, the correct handling of the background gamma-ray emission, which represent a more difficult problematic the higher it is. This contribution focuses on this very point: devising the first ideas for a method of stacking at low Galactic latitudes which not only may allow studying already obtained data (i.e., EGRET), but also be applied to the forthcoming observations.

In the section below we describe the general ideas of the stacking technique performed. In section 3 we comment on the application of this technique to source population studies in the Galactic Plane (GP), specifically in the study of pulsars. Our results are given in section 4. To verify the implication of them, we performed simulations, described in section 5. Finally, a short discussion is given in section 6.

2 The stacking technique

The general stacking method we have applied follows that outlined of reference [3]. In order to perform the stacking technique and look for a possible collective detection of gamma-ray emission above 100 MeV near the GP, we have extracted rectangular sky maps with the selected target objects located at the center. We have used EGRET data from April 1991 through September 1995 —matching the baseline of the Third EGRET Catalog [4], in galactic coordinates. The extracted maps for each particular target were chosen to be 60×60 in size, in order to have large fields of views and be consistent with the EGRET point spread function (PSF). We have transformed the coordinates of each map into pseudo-coordinates, with the target object at the center. After doing this, the maps were co-added, producing the stack-

A. Cillis
Goddard Space Flight Center/NASA
Greenbelt 20771, MD, USA
Tel.: +1-301-286-0977 Fax: +1-301-286-1215
E-mail: cillis@gamma.gsfc.nasa.gov

O. Reimer
W.W. Hansen Experimental Physics Laboratory &
Kavli Institute for Particle Astrophysics and Cosmology
Stanford University
Stanford, CA 94305-4085, USA
Tel.: +1-650-724-6819 Fax: +1-650-725-2463
E-mail: olr@stanford.edu

D. Torres
Institució de Recerca i Estudis Avançats (ICREA) &
Institut de Ciències de l'Espai (IEEC-CSIC)
Facultat de Ciències, Universitat Autònoma de Barcelona
Torre C5 Parell, 2a planta
08193 Barcelona, Spain
Tel.: +34-93-581-4352 Fax: +34-93-581-4363
E-mail: dtorres@ieec.uab.es

ing. It was also necessary to extract a diffuse background map for each target object. For this purpose, we have used the diffuse model that is standard in EGRET analysis [5]. In order to take into account the existence of identified EGRET sources [4,6], idealized sources with the appropriate fluxes distributed following EGRET's PSF as well as the modulated artifacts were added to the diffuse background. On the other hand, the unidentified EGRET sources were not added to the background in this study. It was necessary to normalize each one of the extracted diffuse maps (D_i) for the different exposures (ϵ_i) of the target objects. The extracted diffuse map for each target object was also transformed into pseudo-coordinates. Finally the diffuse maps for the co-added data were obtained as: $1/\epsilon_{total} \sum_i c_i$ where c_i are the counts diffuse maps ($c_i = \epsilon_i D_i$) and $\epsilon_{total} = \sum_i \epsilon_i$. To analyze EGRET data we used the standard likelihood technique based upon gamma ray counts maps that were binned in measured gamma-ray energy and spatially in rectangular projection in Galactic or celestial coordinates [7]. The likelihood function of the EGRET data is the probability of the observed EGRET data for a specific model of high energy gamma-ray emission, and could be written as the product of the probability for each pixel: $L_\theta = \prod_j p_j$, where p_j is the Poisson probability of observing n_j counts in pixel j when the number of counts predicted by the model is θ_j . The logarithm of the likelihood is used in hypothesis testing and is usually more easily calculated. Neglecting the last term (model independent) the logarithm of the likelihood is given by:

$$\log L_\theta = \sum_j [n_j \log(\theta_j) - \theta_j]. \quad (1)$$

The point-source component of the model consists of an "active" source (c_a counts located at (α_a, δ_a)) subject to parameter estimation, and "inactive" sources with fixed counts at fixed positions. Thus, the total model prediction for pixel j is given by

$$\theta_j = g_{mul} G_j + g_{bias} 10^{-5} E_j + c_a PSF(\alpha_a, \delta_a, j) + \sum_k c_k PSF(\alpha_k, \delta_k, j), \quad (2)$$

where c_k is the number of counts for the "inactive" source at (α_k, δ_k) ; $PSF(\alpha, \delta, j)$ is the fraction of the PSF located at (α, δ) that is in pixel j ; E_j is the exposure in pixel j ; and $G_j = \sum_k G_k PSF(\phi_{jk}) / \sum_k PSF(\phi_{jk})$ (where ϕ_{jk} is the angle between pixels j and k). The parameters of the gamma-ray model are estimated via the Maximum likelihood approach. The sum in equation (1) is done for pixels within an adjustable analysis radius (nominally 15° for $E > 100$ MeV). Within this circle, the Galactic diffuse radiation model, is scaled by a multiplier, g_{mul} , which is estimated by maximum likelihood. Also, a maximum likelihood value is used for the level of isotropic diffuse intensity, g_{bias} . This decouples the likelihood point-source analysis from uncertainties in the large-scale diffuse emission model for analyzing point sources in the given region of interest. Only the shape of the model

over the 15° radius circle is used for point-source analysis. The expected value of g_{mul} is 1 and g_{bias} is 0 if the galactic diffuse model is correct. In order to test the significance of a detection, the model of equation (2) is used in the likelihood ratio test by testing the null hypothesis, $c_a = 0$, against the hypothesis that c_a has the estimated value where g_{mul} and g_{bias} have their optimal values for both hypotheses. This formalism produces a "test statistic": $TS = -2(\ln L_0 - \ln L_1)$, where L_1 and L_0 are likelihood values with and without a possible source. $TS^{1/2}$ is roughly equivalent to the standard deviations.

3 Stacking technique applied to Galactic Plane source population

The stacking technique for population studies of gamma-ray sources has been applied for different class of object in several works (for example: radiogalaxies and Seyfert galaxies [3], LIRGs and ULIRGs galaxies [8], clusters of galaxies [9]). All these studies have been so far applied only to high-latitude source populations because of the odds to deal with a dominant and structured diffuse emission. Here, however, we directly step into a new methodology to quantify the systematic biases arising from significant diffuse contributions. We applied this approach in the analysis of EGRET data to study gamma-ray emission from pulsars for energies above 100 MeV.

Pulsars represent astrophysical laboratories for extreme conditions. Their properties such as densities, temperatures, velocities, electric potentials, and magnetic fields associated with these spinning neutron stars give rise to high-energy emission through a variety of mechanisms. Before the launch of CGRO in 1991 only Crab pulsar (PSR B0531+21), Vela pulsar (PSR B0833-45) and Geminga (but not as pulsar in that moment) were known as gamma-ray sources. The instruments on CGRO have detected a total of 7 pulsars with high significance: Crab, B1509-58, Vela, B1706-44, B1951+32, Geminga, and B1055-52. The weakest (PSR B1951+32) has a statistical probability of occurring by chance of $\sim 10^{-9}$. Not all seven are seen at highest energies: PSR B1509-58 is seen only up to 10 MeV by COMPTEL and not at 100 MeV by EGRET. Sensivity for an individual PSR detection is greatly enhanced once studied phase-coherent. The six seen by EGRET all show a double peak in their light curve. In addition to the six high confidence pulsar detection above 100 MeV, three additional radio pulsars may have been seen by EGRET: B1046-58, B0656+14, J0218+4232. These three all have chance probabilities about 5 orders of magnitude less convincing than PSR B1951+32.

More than 1500 radio pulsars are known and it can be expected that this number will continue to grow as more refined detection equipment is used and spatial coverage is expanded. The gamma ray pulsars can be compared to other pulsars in term of the derived physical parameters.

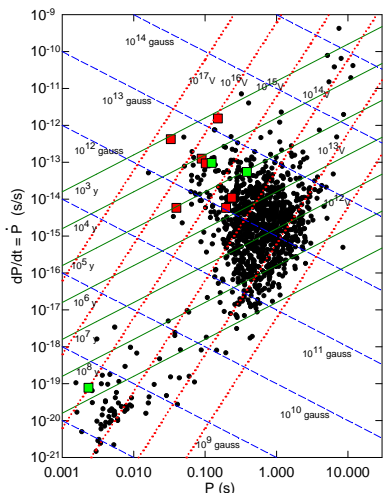


Fig. 1 Distribution of observed radio pulsars in a period-period-derivative diagram derived from ATNF Pulsar Catalogue [11]. The figure is from reference [10]. See text.

Figure 1 (from reference [10]) displays the distribution of observed radio pulsars in a period-period-derivative diagram derived from Australia Telescope National Facility (ATNF) Pulsar Catalogue [11]¹. Lines indicating the "rotational" age of the pulsars and their dipole field strength are also shown as well as the open field line voltage. The gamma-ray pulsars are shown as squares (large dark boxes: seven high-confidence gamma-ray pulsars; large light boxes: three lower-confidence gamma-ray pulsars). Gamma ray pulsars tend to be concentrated in region with high magnetic field (shown by dashed lines), relatively young ages (shown by solid lines) and their open field line voltage is high compared to most pulsars (dotted lines). Efforts to search for additional pulsars in EGRET data have been unsuccessful due to limited statistics. In order to apply the stacking technique in the study of gamma-ray pulsars we created subclasses of pulsars using ATNF pulsar survey after sorting them with different criteria: Surface magnetic flux density ($F_B = 3.2 \times 10^{19} (P/\dot{P})^{1/2}$, where P is the pulsar's period), best estimate of the pulsar distance (D), Spin down energy loss rate (\dot{E}), Energy flux at the Sun (F_E/D^2), Spin down age ($\tau = P/(2\dot{P})$). The classes were chosen accordingly on what is already known about the gamma-ray pulsars that have been detected. We excluded from each list of subclasses those pulsars with $|b| > 30^\circ$ and the detected EGRET pulsars: Crab, J0633+1746, Vela, PSRB1055-52, PSRJ1706-44, PSRB1951+32 (see for example: [12, 13, 10] and also J2229+6114 [14]). Those high-gamma-ray flux pulsars were excluded because they immediately determine the complete stacking problem. We first analyzed pulsars individually using the standard

¹ Figure 1 is from 2003, so pulsars discovered since then are not included.

EGRET software. After that, for each class or subclass we have generated stacked maps containing N pulsars, with $N=2, 4, 6, \dots, 50$. For each stacked map so generated, we have then determined the flux, flux error, upper limit, TS , g_{mul} , g_{bias} , g_{mul}/g_{bias} in the center of the maps and g_{mul}/g_{bias} averaged over a $6^\circ \times 6^\circ$ box, approximately the size of EGRET's PSF for energies > 100 MeV.

4 Results

Figure 2 shows some of the results of our study for all the subclasses of pulsars investigated: \dot{E} , F_B , τ , D and F_E/D^2 . The plots represent the TS obtained (left-axis) and g_{mul}/g_{bias} averaged over $6^\circ \times 6^\circ$ box (right-axis) versus the number of stacked maps. We did not find any signal in the F_E/D^2 class. F_B and τ class both have similar behavior with a peak that appears at high N values in the sample. On the other hand, \dot{E} class has a peak that is dominated from a few sources. The D class is more spread; but a tendency to show high values of TS is apparent perhaps for the more nearby sources, then fading away when distances of about 1 kpc and larger are reached.

During stacking, we keep continuously track on the individual contribution from the diffuse emission model. By comparing the individual contribution and evolution of the diffuse emission over the growing numbers of sources in the stacking sample, we can immediately judge if a change in TS is due to a newly added source or rather to a odd diffuse emission value/problematic treatment during the stacking. There are several cases to distinguish already: (a) steadily accumulating g_{mul}/g_{bias} as in Figure 2 d (D), which points towards an steadily increasing dominance of the diffuse emission, thus diminishing the chance for determine equal TS when adding more sources. (b) constant g_{mul}/g_{bias} as in Figure 2 a, b, c, e - which assures that no glitches in the diffuse model have an impact on the outcome of the stacking result. Initial jumps at the beginning of the stacking are compensated in the average after $\sim 5-6$ sources in sample.

5 Monte Carlo Simulations

In order to understand the results obtained above we ran Monte Carlo Simulation creating fictitious objects with zero gamma-ray flux at random sky positions with $|b| < 30^\circ$, transforming and co-adding the maps, then analyzing the stacked map using the same methods as for real objects. 1000 simulations were performed for 2, 10, 20, 30, and 40 objects added with zero gamma-ray flux. Examples of the results obtained are shown in Figure 3, where the TS cumulative distribution is plotted for 2, 20 and 40 sources added. Accordingly to our results there is no more than 3 % chance of obtaining $TS > 50$

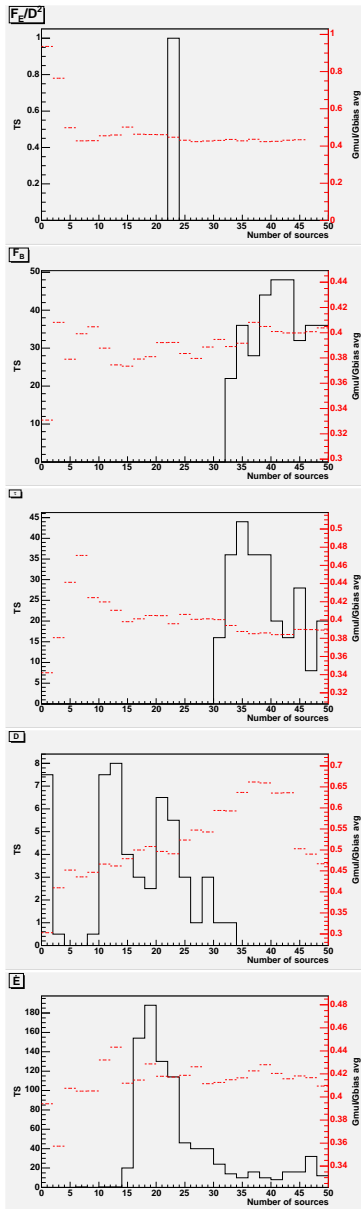


Fig. 2 $TS(g_{mul}/g_{bias})$ versus number of sources added left-axis(right-axis) for different subclasses of pulsars investigated: \dot{E} , F_B , τ , D and F_E/D^2 . TS , solid lines; g_{mul}/g_{bias} , dashed lines. See text.

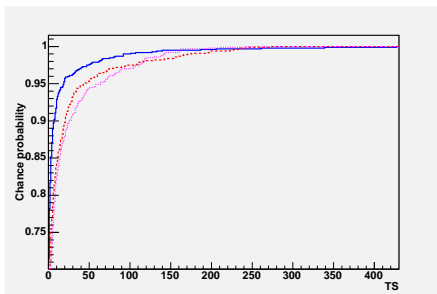


Fig. 3 Monte Carlo Simulations: Chance probability of TS . 2 (solid line), 20 (dashed line) and 40 (dot line) sources added with zero gamma-ray flux. See text.

if 2 sources are added; and no more than 6% if 10 (not shown in Figure 3), 20, 30 (not shown in Figure 3), or 40 objects with zero flux are added randomly in the GP.

6 Discussion

In this paper a new technique to do source population studies using the stacking method in the GP is presented. Different subclasses of pulsars were investigated. Among all orderings of pulsars, the one sorted by distance (D) is the most promising, following the behavior that we expected previous to our study: TS signal fading away when the diffuse contribution grows. The fact that the ordering by F_E/D^2 does not appear to show a signal in the stacking is surprising and will be investigated for systematics in subsequent studies. The F_B and τ classes start to show a signal for quite large number of pulsars, which may be due to the fact that only individual sources affect the stacking. We anticipate that the technique explained in this paper will have application in the study of Galactic sources (not only for PSRs) in GLAST era.

Acknowledgments

DFT has been supported by Ministerio de Educación y Ciencia (Spain) under grant AYA-2006-0530, as well as by the Guggenheim Foundation.

References

1. Torres et al.: Supernova remnants and gamma-ray sources. Phys Report 382, 303 (2003)
2. Romero G., Benaglia P., & Torres D. F : Unidentified 3EG gamma-ray sources at low galactic latitudes. A&A 348, 868 (1999)
3. Cillis A. N., Hartman R. C. & Bertsch D. L.: Stacking Searches for Gamma-Ray Emission above 100 MeV from Radio and Seyfert Galaxies. ApJ 601, 142 (2004)
4. Hartman R. C. et al.: The Third EGRET Catalog of High-Energy Gamma-Ray Sources. ApJS 123, 79 (1999)
5. Hunter S. D. et al.: EGRET Observations of the Diffuse Gamma-Ray Emission from the Galactic Plane. ApJ 481, 205 (1997)
6. Mattox J. R, Hartman R. C. & Reimer O.: A Quantitative Evaluation of Potential Radio Identifications for 3EG EGRET Sources. ApJS 135, 155 (2001)
7. Mattox J. R. et al.: The Likelihood Analysis of EGRET Data. ApJ 461, 396 (1996)
8. Cillis A. N., Torres D. F. & Reimer O.: EGRET Upper Limits and Stacking Searches of Gamma-Ray Observations of Luminous and Ultraluminous Infrared Galaxies. ApJ 621, 139 (2005)
9. Reimer O., Pohl M., Sreekumar P. & Mattox J. R.: EGRET Upper Limits on the High-Energy Gamma-Ray Emission of Galaxy Clusters. ApJ 588, 155 (2003)
10. Thompson D. J.: Gamma Ray Pulsars: Multiwavelength Observations. astro-ph/0312272 (2003)
11. Manchester, R. N., Hobbs, G. B., Teoh, A. & Hobbs, M.: The Australia Telescope National Facility Pulsar Catalogue. Astron. J., 129, 1993-2006 (2005) <http://www.atnf.csiro.au/research/pulsarpsrcat>.

-
12. Fierro J. M., Michelson P. F., Nolan P. L., & Thompson D. J.: Phase-resolved Studies of the High-Energy Gamma-Ray Emission from the Crab, Geminga, and VELA Pulsars. *ApJ* 494, 734 (1998)
 13. Thompson D. J. et al.: Gamma Radiation from PSR B1055-52. *ApJ* 516, 297 (1999)
 14. Thompson D. J., Digel S. W., Nolan P. L., & Reimer O.: Neutron Stars in Supernova Remnants. ASP Conference Proceedings, eds P. O. Slane and B. M. Gaensler (2001), astro-ph/0112518v1